Available online at www.sciencedirect.com
SCIENCE DIRECT®
Journal of Non-Crystalline Solids 351 (2005) 2365–2372
JOURNAL OF NON-CRYSTALLINE SOLIDS
www.elsevier.com/locate/jnoncrysol

Iron doping effect on the electronic structure in yttrium aluminosilicate glasses

V. Simon [a,*], D. Eniu [b], A. Takács [c], K. Magyari [a], M. Neumann [c], S. Simon [a]

[a] Department of Physics, Faculty of Physics, Babes-Bolyai University, M. Kogalniceanu 1, 400084 Cluj-Napoca, Cluj, Romania
[b] Faculty of Pharmacy, University of Medicine and Pharmacy, 400010 Cluj-Napoca, Romania
[c] Department of Physics, University of Osnabrück, 49069 Osnabrück, Germany

Received 6 February 2005; received in revised form 3 July 2005

Abstract

X-ray photoelectron spectroscopy was used to obtain information on local atomic arrangements and electronic structure in Y_2O_3–Al_2O_3–SiO_2 glass system doped with up to 1 mol% Fe_2O_3. Core level photoelectron peaks of Si 2p, Al 2p and O 1s in glasses are symmetric and can be fitted to a single peak, suggesting that there is one kind of site for these elements. Most of the oxygen atoms in the different configurations are of bridging type and, therefore, the contributions to the O 1s core level spectrum from these configurations are undistinguishable. The photopeak symmetry and the binding energies of O 1s electrons show these glasses to be covalent compounds. EPR results indicate that the irons are located in sites subjected to different crystalline field strengths.

PACS: 61.43.Fs; 76.30.Fc; 79.60.Ht

1. Introduction

Yttrium aluminosilicate glasses have led to a special family of glasses used in radiotherapy [1]. Among the oxide materials that are specially developed for medical use, glasses for radiotherapy and hyperthermia are also included. Glasses are used for internal radiotherapy of cancer as radioactive microspheres. The radioisotope Y-90 is activated by neutron irradiation of the initial isotopic stable glasses. The advantage of using these radiation carriers in relation to the conventional external beam radiotherapy is that much larger doses of radiation can be safely delivered to the target site, eliminating exposure to other parts of the body. The application of yttrium oxide aluminosilicate glasses in cancer therapy could be extended from internal radiotherapy to hyperthermia therapy [2] by addition of iron oxide to the yttrium aluminosilicate glass composition. The surface properties influence the biomaterials behavior in the human body and depend on the local atomic arrangement. Spectroscopic techniques like X-ray photoelectron spectroscopy become an important tool in the study of the local structure of oxide glasses [3].

The purpose of this work is to study the electronic structure and implicitly the local order changes in yttrium aluminosilicate glasses doped with iron. The changes depending on Fe_2O_3 content are observed from the X-ray photoemission and electron spin resonance spectroscopic data.

2. Experimental

Glass samples belonging to $17Y_2O_3 \cdot 19Al_2O_3 \cdot (64 - x)SiO_2 \cdot xFe_2O_3$ system ($0 \leqslant x \leqslant 1$ mol%) were

* Corresponding author. Tel.: +40 264 405300; fax: +40 264 591906.
E-mail address: viosimon@phys.ubbcluj.ro (V. Simon).

0022-3093/$ - see front matter
doi:10.1016/j.jnoncrysol.2005.07.010

obtained using oxides of reagent grade purity. According to the phase diagram [4] of SiO_2–Al_2O_3–Y_2O_3 ternary system (Fig. 1), the oxide mixtures that can be melted up to 1600 °C include in their composition range the investigated host glass wherein the iron oxide was added up to 1 mol%. Calculated amounts of these oxide powders were mixed and melted in corundum crucibles at 1550 °C for 30 min. The samples were obtained by fast quenching of the melts cast and pressed between the steel plates at room temperature. X-ray powder diffraction analysis did not show any crystalline phase. The diffraction patterns consist of a very large peak typical of glass systems.

Thermal analysis measurements were carried out using a MOM derivatograph. Thermogravimetric, differential thermogravimetric and differential thermal analysis curves were recorded from powder samples, with a rate of 10 °C/min, up to 1000 °C. The differential thermal analysis curves show no thermal event in the temperature range of the experiment.

XPS measurements were performed using a PHI 5600ci Multi Technique system with monochromatized AlK_α radiation from a 250 W X-ray source ($h\nu = 1486.6$ eV). During the measurements, the pressure in the analysis chamber was in the 10^{-9} Torr range. Low energy electron beam was used to achieve charge neutrality at the sample surface. High resolution core level scans were acquired for the C 1s, Si 2p, Si 2s, Al 2p, Y 3d, Y 3p, Fe 2p and O 1s photoelectron peaks along with the valence band spectra. The absolute binding energies of the photoelectron spectra were determined by referencing to the C 1s transition at 284.6 eV that results most probably during the measurements from adsorbed species. The position and full width at half maximum of photoelectron peaks were estimated using spectra simulation based on summation of lorentzian and gaussian functions.

Electron spin resonance analysis was carried out on powder samples with an ADANI spectrometer, at room temperature, in X band (9.4 GHz) with 4 G modulation amplitude.

The error in the estimation of binding energy and full width at half maximum of photoelectron peaks was around ±0.05 eV. The g factors were estimated from electron paramagnetic resonance spectra with an accuracy of ±0.01.

3. Results

X-ray photoelectron survey scans were taken for each glass sample from fractured surfaces in the binding energy range 0–1400 eV and are shown in Fig. 2. The main photoelectron peaks are identified on the spectra.

High resolution Si 2p spectra are shown in Fig. 3. The binding energies of the Si 2p core level electrons determined from these spectra are encompassed between 100.54 and 101.99 eV and the full width at half maximum ranges from 2.45 to 2.76 eV.

High resolution Al 2p spectra are shown in Fig. 4. The photopeaks are relative narrow, symmetric and show changes in binding energy from 72.79 to 73.70 eV and in full width at half maximum from 2.27 to 2.43 eV as iron oxide content increases from 0.2 to 1 mol%.

The O 1s high resolution spectra shown in Fig. 5 consist of a single relative symmetric peak. The iron doping effect is observed without doubt already for $x = 0.2$. Both binding energy and line width are modified. The binding energy is diminished and the line width is narrowed. By increasing the Fe_2O_3 doping content to 1 mol% binding energy and line width show an apparently linear increase from 529.78 to 530.91 eV, respectively from 2.84 to 3.00 eV.

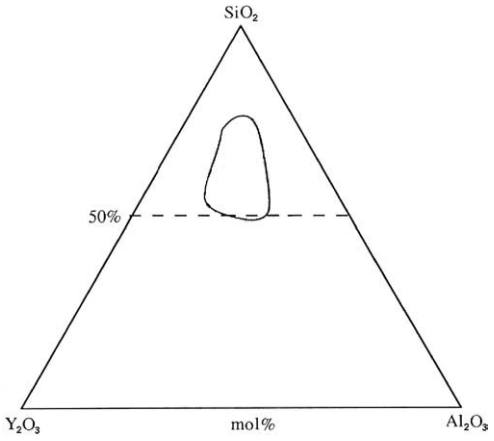

Fig. 1. Glass forming region for SiO_2–Al_2O_3–Y_2O_3 glasses melted at or below 1600 °C according to Ref. [4].

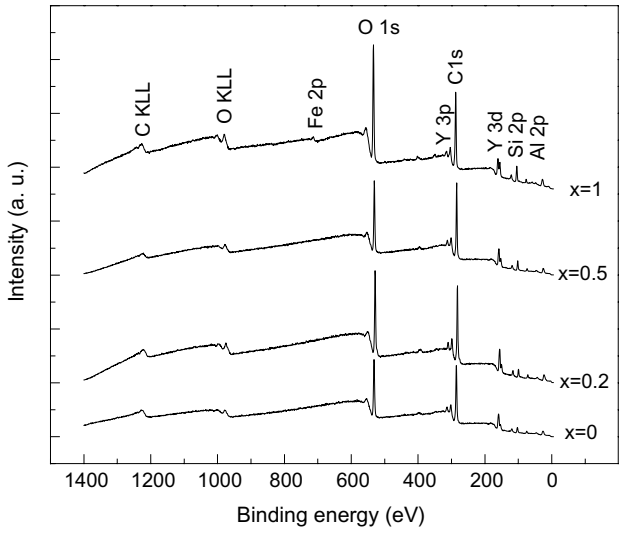

Fig. 2. XPS survey spectra of $17Y_2O_3 \cdot 19Al_2O_3 \cdot (64 - x)SiO_2 \cdot xFe_2O_3$ samples.

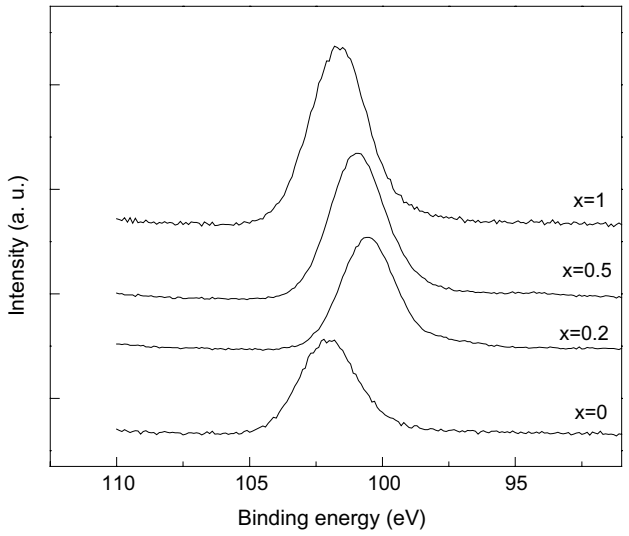

Fig. 3. Si 2p core level photoelectron spectra of $17Y_2O_3 \cdot 19Al_2O_3 \cdot (64 - x)SiO_2 \cdot xFe_2O_3$ samples.

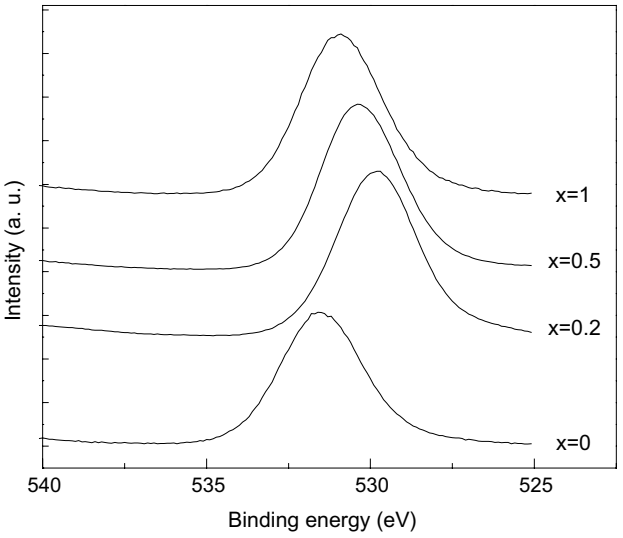

Fig. 5. O 1s core level photoelectron spectra of $17Y_2O_3 \cdot 19Al_2O_3 \cdot (64 - x)SiO_2 \cdot xFe_2O_3$ samples.

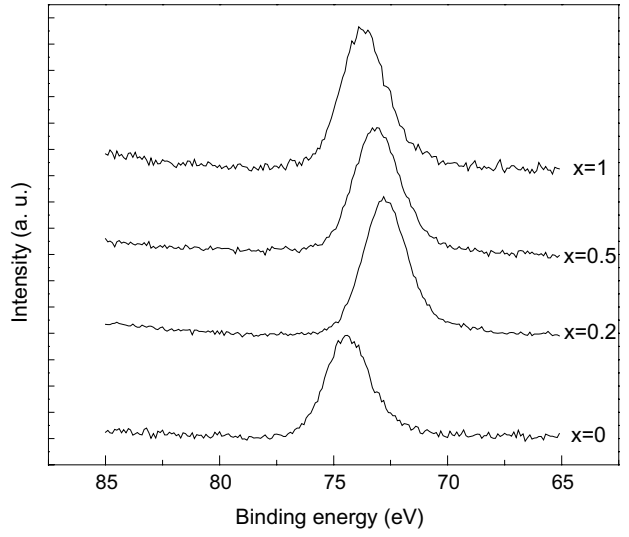

Fig. 4. Al 2p core level photoelectron spectra of $17Y_2O_3 \cdot 19Al_2O_3 \cdot (64 - x)SiO_2 \cdot xFe_2O_3$ samples.

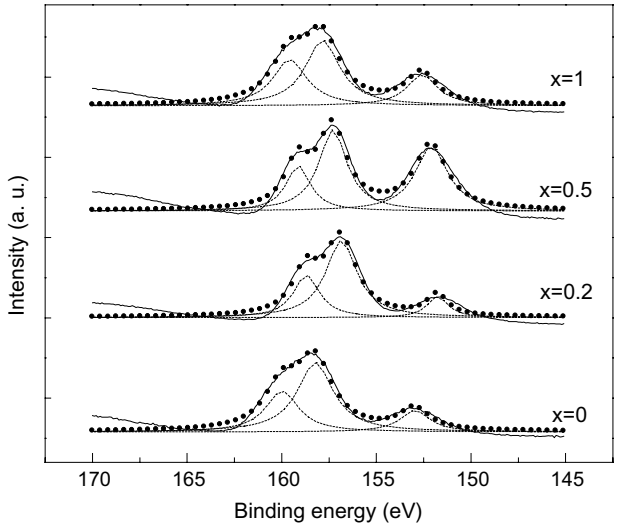

Fig. 6. Experimental and simulated Y 3d and Si 2s core level photoelectron spectra of $17Y_2O_3 \cdot 19Al_2O_3 \cdot (64 - x)SiO_2 \cdot xFe_2O_3$ samples.

In Fig. 6 are shown the high resolution Y 3d and Si 2s spectra, recorded together due to their spectral vicinity. The Y 3d spectra present a spin–orbit splitting of 11.73–1.85 eV. The Si 2s photopeaks are symmetric.

The Y 3p high resolution spectra (Fig. 7) present a spin–orbit splitting close to 11.7 eV. Relative to the host glass sample ($x = 0$), the binding energy of Y 3p photopeaks are slightly lower in the sample with $x = 0.2$ mol% Fe_2O_3, but the binding energy sensibly increases with the doping level.

The Fe 2p core spectra are noisy and split by the 2p spin–orbit effect into the $2p_{3/2}$ and $2p_{1/2}$ peaks (Fig. 8).

The valence band features are generally large (Fig. 9). The spectra present negligible intensity below 2 eV. There are two broad shoulders around 5 and 12 eV.

The environment of Fe^{3+} ($3d^5$, $^6S_{5/2}$) ions was investigated by electron paramagnetic resonance (EPR). The EPR spectrum recorded from the sample with low iron content is dominated by $g = 4.30$ line (Fig. 10). As Fe_2O_3 content increases to 1 mol%, the resonance signal recorded at $g = 2.00$ is well developed in the EPR spectrum.

4. Discussion

The structureless DRX patterns recorded from the prepared samples attested to their vitreous state. The lack of the crystallization peaks in DTA curves proves

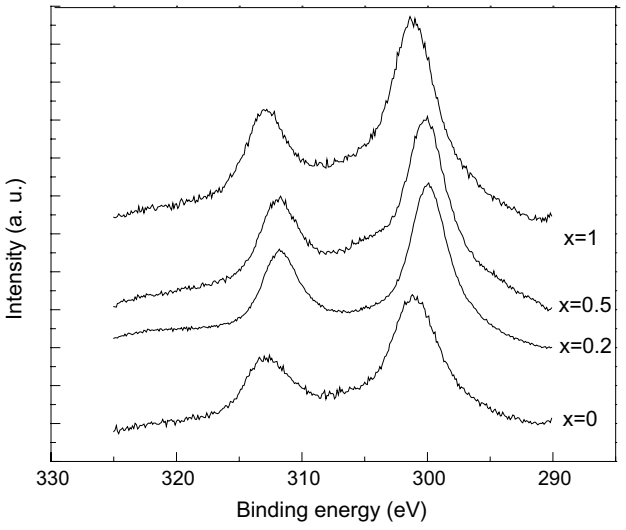

Fig. 7. Y 3p core level photoelectron spectra of $17Y_2O_3 \cdot 19Al_2O_3 \cdot (64 - x)SiO_2 \cdot xFe_2O_3$ samples.

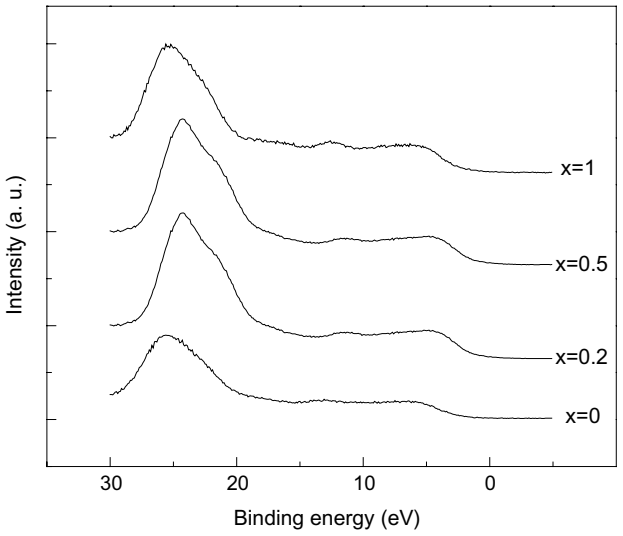

Fig. 9. Valence band spectra of $17Y_2O_3 \cdot 19Al_2O_3 \cdot (64 - x)SiO_2 \cdot xFe_2O_3$ samples.

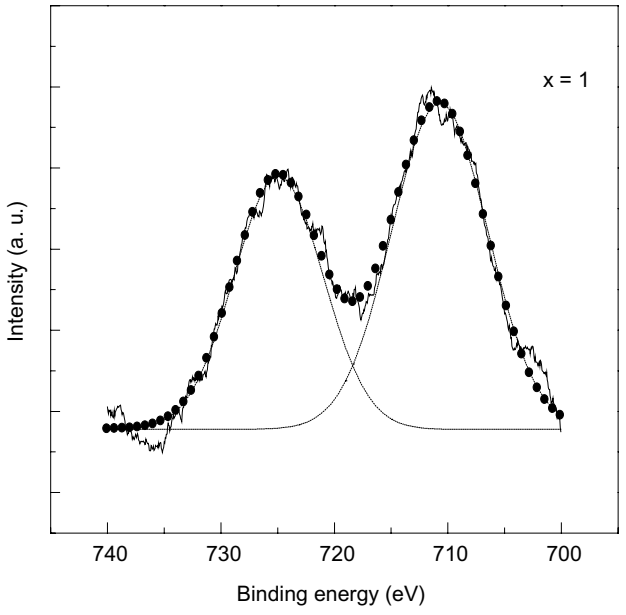

Fig. 8. Fe 2p core level experimental (solid line) and simulated (short dots) photoelectron spectra of $17Y_2O_3 \cdot 19Al_2O_3 \cdot 63SiO_2 \cdot 1Fe_2O_3$ samples.

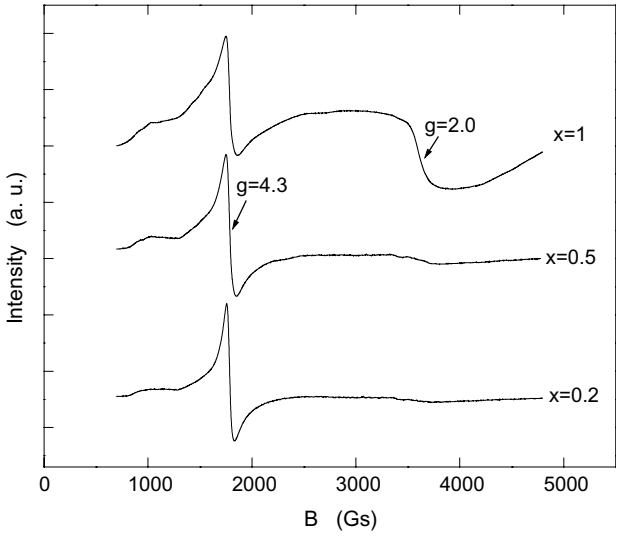

Fig. 10. EPR spectra of $17Y_2O_3 \cdot 19Al_2O_3 \cdot (64 - x)SiO_2 \cdot xFe_2O_3$ samples.

the good glass stability up to 1000 °C versus other silicate glass systems [5].

Pure silica glass is a prototype of a network-forming glass. Its very high melting temperature can be reduced by the addition of modifier oxides. The modifier oxides cause the network to breakdown. The mechanism of this incorporation mainly depends upon the valence state and the coordination of the glass former and modifier elements. In the pure silica glass, there are many small rings that produce a complex and quite rigid three-dimensional network. Opening this network up and altering the ratio between the number of silicon and oxygen atoms produced changes in the local structure and implicitly in the melting temperature.

There are several criteria for predicting the role of the oxides in a glass by considering and comparing the characteristic parameters of the entering cations. In Table 1 are given ionic radius, coordination type, ionic field strength, single bond strength with oxygen and electronegativity of the cations from the investigated glasses [6–8]. The cationic field strength is expressed by the ratio of the cation charge to the square of the ionic radius. The cations belonging to the conventional glass former oxides are characterized by high field strengths as compared to the cations entering as modifiers. In this

Table 1
Coordination number, field strength, Pauling electronegativity and single bond strength for the cations entering in $17Y_2O_3 \cdot 19Al_2O_3 \cdot (64 - x)SiO_2 \cdot xFe_2O_3$ glasses

Cation	Coordination number	Shannon ionic radius (Å) [6,7]	Cation field strength ($Å^{-2}$)	Electronegativity (Pauling units) [8]	Single bond strength M–O (kJ mol^{-1}) [8]
Si^{4+}	4	0.40	25	1.90	799.6 ± 13.4
	6	0.54	13.72		
Al^{3+}	4	0.53	10.68	1.61	511 ± 3
	6	0.675	6.58		
Y^{3+}	6	1.04	2.77	1.22	719.6 ± 11.3
	8	1.159	2.23		
Fe^{3+}	4 Tetrahedral	0.63	7.56	1.83	390.4 ± 17.2
	6 Octahedral	0.69	6.30		
	8	0.92	3.54		
Fe^{2+}	4 Tetrahedral	0.77	3.37		
	4 Square-planar	0.78	3.29		
	6 Octahedral	0.75	3.56		
	6 Octahedral, high spin	0.92	2.36		
	8	1.06	1.78		

approach, one remarks (Table 1) that in the investigated system Al_2O_3, Fe_2O_3 and particularly Y_2O_3 are expected to play the role of modifier oxides in the silicate glass network built up from tetrahedral [SiO_4] structural units.

Several techniques are employed in an attempt to identify the atomic environment of the different elements in glasses. X-ray photoelectron spectroscopy is used to obtain information from the photoelectron peaks corresponding to the component elements [9–11]. As can be seen from Table 2, the binding energies (BE) of the Si 2p (Fig. 3) core level electrons determined from these spectra are lower than 103.4 ± 0.2 eV and the full width at half maximum (FWHM) are larger than 1.45 ± 0.05 eV, the values reported for pure silica glass [12]. This result points out a weaker bond of silicon atoms in SiO_2–Al_2O_3–Y_2O_3 system and a disorder degree higher than in the pure silica glass. Inspecting the FWHM values as a function of iron doping level (Table 2), one remarks that the lines become slightly narrower by iron doping, indicating an ordering tendency in the local structure of the host yttrium aluminosilicate glass.

The binding energies of Si 2p core level electrons after an initial decrease gradually change to higher values as Fe_2O_3 content increases, since some of the Si–O–Si bonds are changed into Si–O–M bonds. As the charge distribution in the Si–O–Si bond is displaced towards the oxygen atom, there is a deficiency in electron density around the Si atom, causing increase in binding energy of Si 2p core level electrons. This chemical shift is caused by the partial transfer of electrons from Fe^{3+} to O^{2-} ions.

The same composition dependence is observed for Al 2p, Y 3d and Y 3p core level photopeaks. This is correlated with the fact that the effective electronic charge density on a cation (silicon, aluminum, yttrium) decreases as the number of oxygen anions increases. The decrease in effective electronic charge density around the cations would be reflected in an increase in the binding energy of the remaining electrons. In the high resolution Al 2p spectra (Fig. 4) relative narrow and symmetric photopeaks are recorded. The Al 2p peaks exhibit a gaussian shape that indicates, in the limits of XPS methods, only one type of surrounding for Al atoms. For the sample without iron, the binding energy of 74.41 eV corresponds to that of alumina. The broadening of the Al 2p by progressive iron addition may be caused by the deformation of aluminum polyhedra [13] assumed to be preponderantly tetracoordinated as have been shown by ^{27}Al MAS NMR investigation of other yttrium-alumino-silicate glasses [14,15].

Table 2
Core level electron binding energies (BE) and full width at half maximum (FWHM) for Si 2p, Al 2p and O 1s photoelectron peaks of $17Y_2O_3 \cdot 19Al_2O_3 \cdot (64 - x)SiO_2 \cdot xFe_2O_3$ samples

x (mol%)	Si 2p		Al 2p		O 1s	
	BE (eV)	FWHM (eV)	BE (eV)	FWHM (eV)	BE (eV)	FWHM (eV)
0	101.99	2.76	74.41	2.33	531.54	2.94
0.2	100.54	2.49	72.79	2.27	529.78	2.84
0.5	100.95	2.45	73.17	2.39	530.31	2.89
1	101.63	2.50	73.70	2.43	530.91	3.00

Fig. 5 shows the O 1s high resolution spectra. The binding energies are in the range reported for silicate glasses [3,16]. In the XPS studies of oxide glasses, the binding energy of O 1s electrons in oxygens bonded to different cations seems to be the most informative measurement with respect to the structure of the glass [17]. This binding energy is a measure of the extent to which electrons are localized on the oxygen or in the internuclear region and hence of the constraints on the network, reflected by the physical properties. The terms network former, intermediate, and modifier are therefore simply a reflection of this electron localization. A modifier cation has low electronegativity and forms ionic bonds and there is a transfer of electronic charge to the neighboring oxygen. This increase in electron density at the oxygen atoms means that the electron binding energies are reduced and this is reflected in the photoelectron spectrum, giving rise to non-bridging oxygen peak. According to the classical model of silicate glasses, the influence of the network modifier cations on the local structure consists in the compensation of the negative charges and is responsible for the disruption of the oxygen bridges in the silica network [18]. A network former has relatively high electronegativity, the bond to oxygen is more covalent, constraining the electron density to the region between the atoms and reducing the electron density on the oxygen atom. This results in an increased electron binding energy, which yields a bridging oxygen peak in the XPS spectrum. In our samples, the O 1s peak is well simulated with a single peak. This would indicate that electrons on the oxygen atoms in the different configuration have similar binding energies. The binding energy dependence on Fe_2O_3 content is similar with the evolution determined in zinc borate glasses by addition of Pr_2O_3 [19].

The O 1s core level peaks for all Fe_2O_3 doping levels are symmetric, indicating that the environments around the oxygen atoms are undistinguishable. It is considered that these yttrium aluminosilicate glasses consist of SiO_4 polyhedra and MO_n (where M = Al, Y) polyhedra sharing corners according to the glass formation rules. As has been shown by nuclear magnetic resonance results [14,15] aluminum atoms are mainly tetracoordinated and only a small amount of them are penta- and much less hexacoordinated. The MO_n and SiO_4 are therefore connected by Si–O–Si and M–O–Si linkages, because the cations have comparable single bond strength (Table 1) and can therefore substitute for each other in bonding with O atoms. The M–O distances can be modified in different glass hosts [20], which can be related to the different structural role of the element M in the glass structure. X-ray and neutron diffraction data obtained for other aluminosilicate glass systems are consistent with the hypothesis that silicon and aluminum occupy tetrahedral sites and for certain compositions silicon can enter the aluminate network [21]. The ordering behavior of cations in aluminosilicate glasses and implicitly the short-range order of framework cations can be also approached with respect to the Al–O–Al avoidance principle, which postulates that the Al–O–Si linkage is energetically more favorable than the combination of Si–O–Si and Al–O–Al [20,22].

Dimitrov and Komatsu [23] proposed a simple oxide classification on the basis of correlation between electronic polarizabilities of the ions and their binding energies determined by XPS. The classification takes into account two different physical properties of the oxide ion, electronic polarizability and O 1s binding energy. The O 1s binding energies for the investigated samples range from 529.8 to 531.54 eV (Table 2). According to Dimitrov and Komatsu's model and regarding their high symmetric O 1s core level photopeak they could be considered covalent compounds.

From Fig. 6 one can observe the iron doping influence both on yttrium and silicon neighbors. The Si 2s photopeaks, like Si 2p ones (Fig. 3) are symmetric. The data of Table 3 show that Si 2s binding energy and line width are in the same evolution with the Fe content as for Si 2p photopeak (Table 2).

By inspecting the Y 3d photopeaks one remarks that they are not symmetric and for $x = 0.2$ and 0.5 is evident the spin–orbit splitting. On deconvolution they have been found to consist of two peaks each. Using the values of the areas under the lines corresponding to the deconvoluted spectra, we consider that the ratio between the area of yttrium and silicon peak recorded in the same spectrum could reflect the differentiated influence of iron doping on the local order in their atomic environment containing these elements. The positions of the photoelectron peaks are shifted to some higher energies relative to pure Y $3d_{5/2}$ (155.8 eV) and Y $3d_{3/2}$ (157.7 eV).

The Y 3p high resolution spectra (Fig. 7) present a spin–orbit splitting close to 11.7 eV. The positions of the photoelectron peaks (Table 4) are shifted to some higher energies relative to elemental yttrium characterized by Y $3p_{3/2}$ (298.8 eV) and Y $3p_{1/2}$ (310.6 eV).

Due to the low atomic concentration of Fe_2O_3 in the studied samples, the iron spectra present a rather high signal-to-noise ratio. The smoothed experimental and simulated spectrum of the sample doped with 1% mol Fe_2O_3 is shown in Fig. 8. The binding energies for Fe 2p in this system are shifted to higher values in comparison to pure iron (Fe $2p_{3/2}$ – 706.8 eV and Fe $2p_{1/2}$ – 719.9 eV).

The valence band spectra (Fig. 9) are related to the density of occupied electronic states in the valence band. They are generally large and consist of peaks from O 2p and Si 3s, Si 3p and Al 3s, Al 3p molecular orbitals [3,24] and there is a slight shift to lower binding energy on introducing Fe_2O_3. The spectra present negligible intensity below 2 eV, which correspond to the top of the

Table 3
Core level electron binding energies (BE), full width at half maximum (FWHM), spin–orbit splitting and areas (A) under simulated lines for Si 2s, Y $3d_{5/2}$ and Y $3d_{3/2}$ photoelectron peaks from $17Y_2O_3 \cdot 19Al_2O_3 \cdot (64 - x)SiO_2 \cdot xFe_2O_3$ samples

x (mol%)	BE (eV)	FWHM (eV)	BE (eV)		Spin–orbit splitting (eV)	$A_{(Y\,3d)}$ (a.u.)	$A_{(Si\,2s)}$ (a.u.)	$A_{(Y\,3d)}/A_{(Si\,2s)}$
	Si 2s	Si 2s	Y $3d_{5/2}$	Y $3d_{3/2}$				
0	152.95	2.13	158.18	159.91	1.73	238.09	38.66	6.16
0.2	151.77	1.97	156.86	158.71	1.85	219.68	29.96	7.33
0.5	152.21	2.37	157.28	159.11	1.83	211.54	131.99	1.7
1	152.71	2.35	157.84	159.57	1.73	239.35	58.88	4

Table 4
Core level electron binding energies (BE), full width at half maximum (FWHM), spin–orbit splitting and areas (A) under simulated lines for Y $3p_{3/2}$ and Y $3p_{1/2}$ photoelectron peaks from $17Y_2O_3 \cdot 19Al_2O_3 \cdot (64 - x)SiO_2 \cdot xFe_2O_3$ samples

x (mol%)	BE (eV)		FWHM (eV)		Spin–orbit splitting (eV)	A (a.u.)		$A_{3/2}/A_{1/2}$
	Y $3p_{3/2}$	Y $3p_{1/2}$	Y $3p_{3/2}$	Y $3p_{1/2}$		Y $3p_{3/2}$	Y $3p_{1/2}$	
0	301.17	312.95	5.29	5.27	11.68	285.17	146.19	1.95
0.2	300.03	311.80	3.51	4.56	11.77	239.46	158.29	1.51
0.5	300.13	311.80	4.90	6.21	11.67	360.78	238.76	1.51
1	301.18	312.86	5.13	5.85	11.68	416.95	241.66	1.73

valence band. This is an indication that the investigated system is non-conductive. There are two broad shoulders around 5 and 12 eV, which could be assigned to mixed molecular orbitals Al 3sp (0 eV)–O 2p (7.8 eV) with mostly O 2p character [24,25]. The shoulder at lower binding energy could be assigned to π bonding orbitals and the second one to σ bonding orbitals [26]. In the valence band spectra O 2s peaks also occur [27,28]. The photopeak around 25.5 eV corresponds to O 2s core level electrons. Its binding energy is shifted to lower values by doping with iron oxide.

The energetic state of Fe^{3+} ions with the spin magnetic moment $\vec{S}$ in an external magnetic field $\vec{B}$ can be described using the Hamiltonian [29]:

$$\mathscr{H} = g_0\beta\vec{B}\vec{S} + D\left[S_z^2 - \frac{1}{3}\cdot S(S+1)\right] + E(S_x^2 - S_y^2),$$

where the first term is Zeeman term and the following are the second order terms of the interaction with the crystalline field. D and E are the axial and rhombic constants of the energy level splitting in the zero magnetic field.

For very low Fe_2O_3 contents the EPR spectrum (Fig. 10) is dominated by $g = 4.30$ line. This line is assigned to Fe^{3+} ions in sites of low symmetry, characterized by strong crystalline field [30]. As Fe_2O_3 content increases to 1 mol%, in the EPR spectrum is well developed the resonance signal recorded at $g = 2.00$. This signal is arising from Fe^{3+} ions which are dipolar interacting and are disposed in sites of octahedral symmetry, in weak crystalline fields, characteristic for structural relaxed sites.

5. Conclusions

Iron doping effect on the binding energies of core level electrons of the cations entering the investigated glasses was correlated with changes in the next nearest neighbors of the cations. The full width at half maximum indicates an ordering tendency in the local structure by iron addition to the host yttrium aluminosilicate glass. Progressive iron doping causes the decrease of the effective electronic charge density on the other cations. Valence band data show that the system is non-conductive.

The oxygen atoms in the different configurations are of bridging type and therefore their contributions to the O 1s core level spectrum are undistinguishable. The binding energy and the symmetry of O 1s photopeaks show the covalent character of the bonds formed in these glasses. It is assumed that beside the SiO_4 structural units the glass network also contains AlO_4 units. The yttrium and iron act as glass network modifiers. EPR results indicate that the iron is disposed on sites of different crystalline field strengths, depending on the doping level.

References

[1] G.J. Ehrhardt, D.E. Day, Nucl. Med. Biol. 14 (1987) 233.
[2] S. Atalay, H.I. Adiguzel, F. Atalay, Mater. Sci. Eng. A 304 (2001) 796.
[3] I.A. Gee, D. Holland, C.F. McCoville, Phys. Chem. Glasses 42 (2001) 339.
[4] J.E. White, D.E. Day, Key Eng. Mater. 94&95 (1994) 181.

[5] A.A. Cabral, A.A.D. Cardoso, E.D. Zanotto, J. Non-Cryst. Solids 320 (2003) 1.
[6] R.D. Shannon, Acta Cryst. A 32 (1976) 751.
[7] J.E. Huheey, E.A. Keiter, R.L. Keiter, Inorganic Chemistry: Principles of Structure and Reactivity, 4th Ed., HarperCollins, New York, USA, 1993.
[8] J.A. Kerr, in: D.R. Lide (Ed.), CRC Handbook of Chemistry and Physics, 81st Ed., CRC Press, Boca Raton, FL, USA, 2000.
[9] S. Matsumoto, T. Nanba, Y. Miura, J. Ceram. Soc. Jpn. 106 (1998) 415.
[10] R.K. Brow, R.J. Kirkpatrick, G. Turner, J. Am. Cer. Soc. 73 (1990) 2293.
[11] T. Honma, R. Sato, Y. Benino, T. Komatsu, V. Dimitrov, J. Non-Cryst. Solids 272 (2000) 1.
[12] V. Simon, H. Bako-Szilagyi, M. Neumann, S.G. Chizbaian, S. Simon, Mod. Phys. Lett. B 17 (7) (2003) 291.
[13] A. Novosselov, A. Pajaczkowska, E. Talik, Cryst. Res. Technol. 36 (2001) 859.
[14] J.T. Kohli, J.E. Shelby, J.S. Frye, Phys. Chem. Glasses 33 (1992) 73.
[15] T. Schaller, J.F. Stebbins, J. Phys. Chem. B 102 (1998) 10690.
[16] P.C. Soares, P.A.P. Nascente, E.D. Zanotto, Phys. Chem. Glasses 43 (2002) 143.
[17] A. Mekki, Arab. J. Sci. Eng. 28 (1A) (2003) 74.
[18] E. Muller, K. Heide, E.D. Zanotto, Z. Kristallogr. 200 (1992) 287.
[19] G. Speranza, M. Ferrari, M. Bettinelli, Philos. Mag. B 79 (1999) 2145.
[20] S.K. Lee, J.F. Stebbins, Am. Mineral. 84 (1999) 937.
[21] L. Cormier, G. Calas, S. Creux, P.H. Gaskell, B. Bouchet-Fabre, A.C. Hannon, Phys. Rev. B 59 (1999) 13517.
[22] L. Cormier, D.R. Neuville, G. Calas, J. Non-Cryst. Solids 274 (2000) 110.
[23] V. Dimitrov, T. Komatsu, J. Solid State Chem. 163 (2002) 100.
[24] S. Thomas, P.M.A. Sherwood, Anal. Chem. 64 (1992) 2488.
[25] B. Vincent Crist, Handbooks of Monochromatic XPS Spectra, in: Handbook of The Elements and Native Oxides, XPS International, 1999.
[26] C.A.M. Pereira, M. Abbate, W.H. Schreiner, M.A.S. Boff, S.R. Teixeira, J.E. Schmidt, Solid State Commun. 116 (2000) 457.
[27] S. Rondon, P.M.A. Sherwood, Surf. Sci. Spectra 5 (1998) 97.
[28] G. Silversmit, G. De Doncker, R. De Gryse, Surf. Sci. Spectra 9 (2002) 21.
[29] D.L. Griscom, J. Non-Cryst. Solids 40 (1980) 211.
[30] S. Simon, R. Pop, V. Simon, M. Coldea, J. Non-Cryst. Solids 331 (2003) 1.